Asian Journal of Chemistry; Vol. 30, No. 9 (2018), 2151-2158

ASIAN JOURNAL OF CHEMISTRY

https://doi.org/10.14233/ajchem.2018.21500

Spinel Organic-Framework Wrapped Polymer Electrodes for Super Capacitors

GUNJANA CHAUDHARY, ASHOK K. SHARMA*, INDU KAUSHAL and PRIYA SAHARAN

Thin Film Laboratory, Department of Materials Science & Nanotechnology, Deenbandhu Chhotu Ram University of Science & Technology, Murthal-131 039, India

*Corresponding author: E-mail: aksharma210@gmail.com

Received: 5 June 2018; *Accepted*: 12 July 2018; *Published online*: 31 July 2018; AJC-19035

This work presents the blueprint for design and fabrication of novel electrode material by facile thin layer deposition of poly(aniline) (PANI) on highly conductive Mn-doped cobalt ferrite grown on the surface of carbon nanofibers to achieve high specific capacitance for application in energy storage and conversion devices. The crystalline growth of metal oxide over carbon nanofibers uniquely served as a highly conductive template with redox active sites. Physical and chemical aspects of fabricated composites were characterized by FTIR spectroscopy, UV spectroscopy, XRD, FESEM, EDS, HRTEM technique and selected area electron diffraction characterization studies. The electrochemical proficiency of synthesized electrode materials was tested by application of three-electrode system for cyclic voltammetry, galvanostatic charge-discharge and electrochemical impedance spectroscopy. The uppermost specific capacitance of 1866 F g^{-1} at a scanning rate of 5 mV s^{-1} and 1450 F g^{-1} at a current density of 0.75 A g^{-1} were accomplished in aqueous solution of 1 M H_2SO_4 with good cycle stability.

Keywords: Polyaniline, Voltammetry, Composites, Charge-discharge, Impedance.

INTRODUCTION

Polymers in conductive form have come forth as sophisticated electrode materials for energy storage appliances *viz*., super-capacitors [1-4]. Out of the various polymers available polyaniline (PANI) has been studied enormously leading towards superior conductivity, simplified synthesis, appreciable biological stability and cost effectiveness [5-8]. Inspite of these expected characteristics this pseudo-capacitive material hindered by a major restriction of mechanical declination in doping and de-doping operation, which obstructs its performance [9].

Another type of pseudo-capactive electrode materials for high performance capacitor is metal oxides like manganese oxide, nickel oxide, zinc oxide, *etc*. [10-12]. Studies have unveiled that mixed binary transition metal oxides shows enhanced capacitive activity in comparison to lone metal oxides [13-15]. In recent times, spinel metal oxides appeared as a promising pseudo-capacitive electrode material. They offer attributes namely cost effectiveness, enhanced conductivity, environment supportivity, proficient reduction-oxidation and high specific capacitances. Binary metal oxide is assumed to display better redox chemistry over the two individual elemental metal oxides, it is because of synergistic contributions from both the metal ions [16,17]. Many efforts have been made to synthesize composites of spinel metal oxides to attain better electrochemical performance. Wang *et al*. [18] have published electrostatic fabrication of $NiCo_2O_4$-graphene sheets having a specific capacitance of 835 F g^{-1}. Synthesis process and capacitive aspects of cobalt/nickel metal oxide with CNT based materials were given by Fan *et al*. [19]. Xin *et al*. [20] developed nickel and cobalt binary oxide/CNTthin layer film electrochemically and studied the nano-porous morphology and charge-discharge properties. Deng *et al*. [21] reported the preparation of $CoFe_2O_4$ nano-rods and nano-rings and its electrochemical properties [21]. Although, it was detected that pure spinel metal oxides performance cannot be produced to satisfy the performance. A promising vision to upgrade the performance is designing novel spinel metal oxide-based hybrids. The combination of binary hybrids composed of PANI and transition metal oxides can provide enhanced specific capacitance and improved electrochemical performance [22-24]. Also, doping of spinel metal oxides by various transition metal ions is found to tailor its properties. However, few studies about spinel metal oxide/polymer based composites have been reported till now.

Porous carbon based materials have been induced within the reinforcing matrix to add on properties *viz*. enhanced mechanical firmness, large surface area, electrochemical conduct and improved cyclic stability [25-29]. Carbon nanofibers (CNF) are 1-D porous nanomaterials containing carbon framed skeletal structure. They are less expensive and disperse readily than single walled and multi-walled carbon nanotubes. They offers modified mechanical, morphological, electrothermal and reinforcement aspects which shape them advanced filler stuff for carbon electrodes [30,31]. Here in this study, we present a proficient creation of PANI grafted Mn-doped cobalt ferrite/CNF composites through 2-step method. The composites comprising PANI-coated over Mn-doped cobalt ferrite encapsulated carbon nanofibers substrate are presented as superior materials for energy storage resulting from their special morphology and outstanding electro-capacitive performance.

EXPERIMENTAL

Aniline (99%, E. Merck) was distilled twice before further use. Carbon nanofibers having diameter 10-12 nm and length 1 μm was purchased from Sigma Aldrich. Poly(vinylidene fluoride) (PVDF) and activated charcoal were also procured from Sigma Aldrich. All other chemicals such as ammonium persulfate, N,N-dimethyl formamide, ethanol, ammonia solution, $MnCl_2{\cdot}4H_2O$, $CoCl_2{\cdot}6H_2O$ and $FeCl_3{\cdot}6H_2O$ were of ACS grade procured from S.D. Fine Chem. Ltd. Ultrapure water generated from Milli-Q plus system (Millipore Co.) was exclus-ively utilized in preparing all aqueous solutions and rinsing purpose.

Synthesis (step-1): Acid treated carbon nanofiber was obtained by refluxing carbon nanofiber with 100 mL solution of sulfuric acid with nitric acid (1:3 v/v) for 2 h. This product was procured by filtration then washed repeatedly with deionized water and dried for further usage. The obtained carbon nanofiber (0.04 g) was ultrasonicated in 60 mL of absolute ethanol for 1 h. To this reaction mixture $MnCl_2{\cdot}4H_2O$ (0.05 M), $CoCl_2{\cdot}6H_2O$ (0.2 M) and $FeCl_3{\cdot}6H_2O$ (0.4 M) were added and vigorous stirring was done for 0.5 h. Dropwise NH_4OH was added until the pH of the reaction mixture became ~11. The mixture as obtained was seal packed into an autoclave and heated for 20 h at 200 ºC for 20 h. The product obtained was filtered, rinsed properly with deionized water and dried under vacuum at 60 ºC for 10 h. The product was labeled as CF.

Step-2: The extracted CF composite and aniline (1 M) were well stirred to achieve dispersion in 1 M HCl solution. Ammonium persulfate (1 M), freshly prepared in 1 M HCl solution was added to above reaction mixture dropwise and with continuous stirring in an ice bath. The stirring was continued for 10 h in ice cooled water bath to carry out complete polymerization process. Finally, the product labeled as CFP was procured by filteration, followed by washing and drying at 60 ºC under vacuum. The binary CNF/PANI (PF) composite was synthesized *via* a parallel scheme without adding in $MnCl_2{\cdot}4H_2O$, $CoCl_2{\cdot}6H_2O$ and $FeCl_3{\cdot}6H_2O$. Also, Mn-doped cobalt ferrite (MO) was prepared for comparison. Schematic diagram of composite fabrication is exhibited in Fig. 1.

Characterization: IR spectrum through Fourier transform infrared spectrophotometer (FTIR, Perkin Elmer, 90776, KBr pellet) was obtained for structural classification of synthesized composites. The Shimadzu UV-(2450) spectrophotometer was used for examining UV-visible spectrum of composites. Powder X-Ray diffraction was studied on (Phillips Xpert Pro) with CuKα radiation (1.54060 Å, 45 KV voltage). Morphological analysis was made by using field-emission scanning electron microscope (FESEM, Carl Zeiss EVO40), energy dispersive X-ray spectroscopy (EDX, Carl Zeiss EVO 50) and high resolution transmission electron microscopy (HRTEM, TechnaiG2 30STWIN). AutolabPGSTAT (86472) has been employed for cyclic voltammetry, galvanostatic charge-discharge cycles and electrochemical impedance analysis.

Electrochemical measurements: Electrochemical proficiency of composites was evaluated in 1 M H_2SO_4 electrolyte was tested at room temperature in a three-electrode cell assembly, in which a platinum wire used as counter electrode and Ag/AgCl were used as reference electrode. The working electrode was fabricated by compressing a mixture of synthesized composite, conductive agent activated charcoal and binder poly(vinyldiene flouride) (PVDF). The optimized ratio by wt % of coating slurry is comprised of composite material (70 %), activated carbon (20 %) and PVDF binder (10 %) dissolved in dimethyl formamide by using brush coating onto a graphite sheet with a dimension of 1 cm × 1 cm.

RESULTS AND DISCUSSION

FTIR analysis: The MO, CF, PF and CFP nanostructure were analyzed using FTIR spectroscopy. The intense band at 480 cm^{-1} and very weak band at 520 cm^{-1} in the spectrum of MO are observed, which corresponds to intrinsic stretching vibrations of metal-oxygen at octahedral and tetrahedral site, respect-

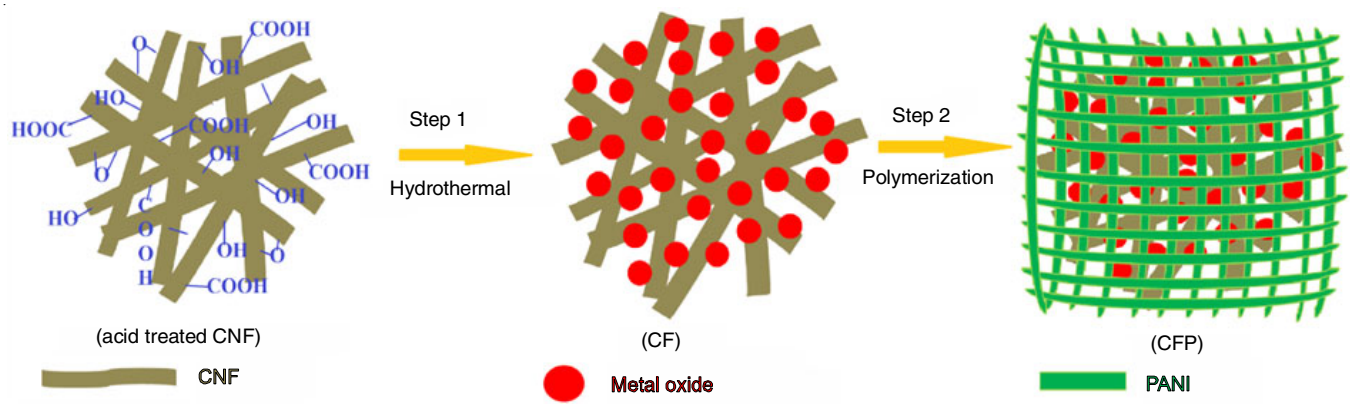

Fig. 1. Schematic illustration for the synthesis of CF and CFP composites

ively (Fig. 2). These IR absorption bands are the characteristic bands of spinel ferrites [32,33]. For CF sample, the presence of different functional groups was found at 1560, 1400, 1090 cm^{-1}, which are attributed to skeletal C=C, C-H and C-OH stretching vibrations (Fig. 2). Due to the interactions between carbon nanofiber and cobalt ferrite, the absorption band corresponding to metal-oxygen stretching vibration is shifted to 595 cm^{-1} [31]. FTIR spectrum of PF shows typical bands of PANI. A band at 3430 cm^{-1} is due to N-H stretching vibrations. Absorption bands at 1601 and 1453 cm^{-1} corresponds to quinoid and benzenoid ring vibrations, respectively. These bands confirm the existence of emeraldine form of PANI. The intense band at 1124 cm^{-1} is related to the conductivity of PANI and is attributed to strong π-π interactions within the conjugated PANI and carbon nanofiber frameworks. Two bands at 2921 and 2861 cm^{-1} refers to asymmetric and symmetric C-H stretching ring vibrations. The absorption band at 881 cm^{-1} is assigned to aromatic C-H out of plane bending vibrations [34-39]. All these absorption bands are noted again in CFP spectrum but with shifted wavelengths and varied intensities (Fig. 2). These results revealed that CF is packed successfully by PANI and there are σ-π interactions among them. PANI has σ and π^* molecular orbitals which overlaps with the empty and filled *d*-orbitals of Fe^{3+} to form σ and π bonds, respectively [40]. In addition, hydrogen bonding interactions between PANI and cobalt ferrite/CNF substrate surface builds a robust structure of the composite.

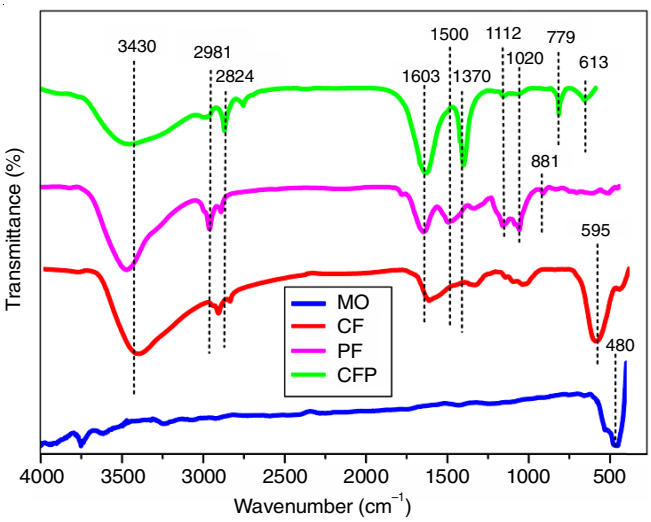

Fig. 2. FTIR spectrum of MO, CF, PF and CFP composites

UV-visible spectroscopy: UV spectroscopy was employed to determine the interfacial interactions among the various components of the synthesized products. The PANI contains two major peaks in spectrum at 335 and 630 nm, which are referred respectively with π-π^* transition of benzene ring and quinoid ring (Fig. 3). A small peak at 462 nm can correspond to polaron-π^* transition [41,42]. MO displays absorbance peak at 260 nm is attributed to charge transfer interactions in cobalt ferrite [43]. Similar absorbance peak is observed in the spectrum of CF which confirms interaction between cobalt ferrite and carbon nanofibers. Spectrum of composite CFP has all the peaks characteristic of PANI as well as of cobalt ferrite which further confirms the incorporation of binary CF embedded in PANI matrix. These bands also accompany the shifting in the peaks and absorbance. Absorbance bands are shifted at 263, 341 and a broad peak at 623 nm in the spectrum of CFP composite (Fig. 3).

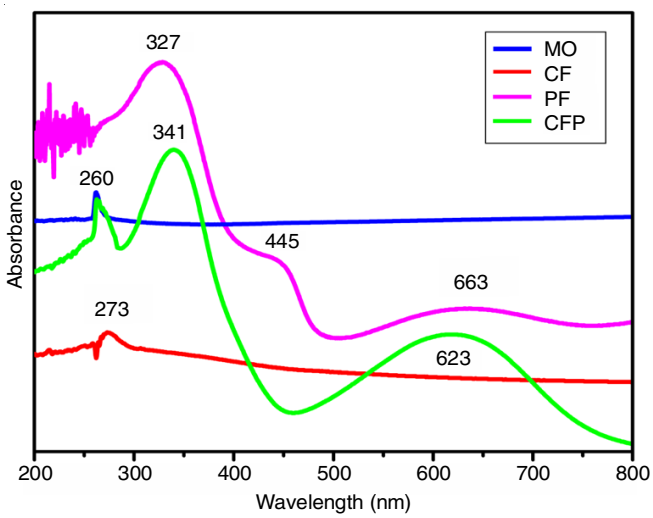

Fig. 3. UV-visible spectra of MO, CF, PF and CFP composites

X-Ray diffraction analysis: XRD diffraction patterns were considered to study the crystalline structure of the composite's surface. The bands are observed for MO can be indexed to (311), (400) and (511) crystal planes of spinel type structure of cobalt ferrite (JCPDS22-1086) [32].Corresponding similar bands are also found (Fig. 4) for the spectrum band of CF with additional peak at 2θ = 25° that corresponds to carbon nanofibers [44]. PF displays only one broad peak at 2θ = 25.5° indexed to (020) crystal plane of doped PANI [45,46]. In the XRD pattern of CFP composite the diffraction bands corresponding to both of MO and PANI can be monitored (Fig. 4). This depicts the successful incorporation of CF in PANI matrix.

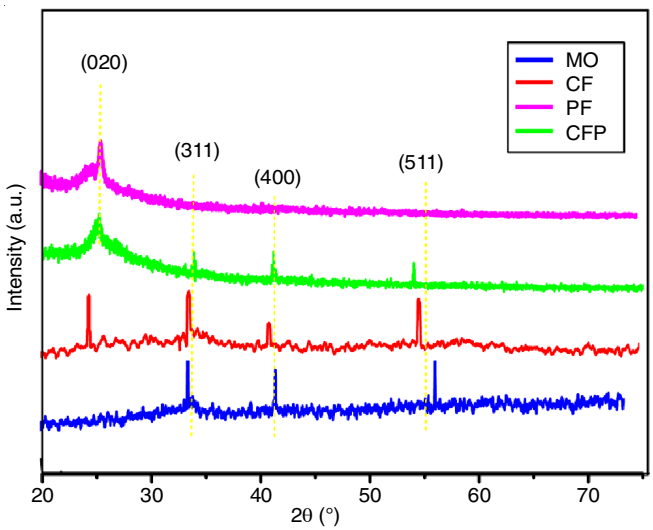

Fig. 4. X-ray diffraction patterns of MO, CF, PF and CFP composites

Morphological analysis: FESEM micrographs have been obtained to examine the surface morphology of fabricated composites. Fig. 5a shows almost uniformly distributed spherical particles of cobalt ferrite with soft agglomeration. Spheres are dense and distributed regularly over the whole area. Fig. 5b

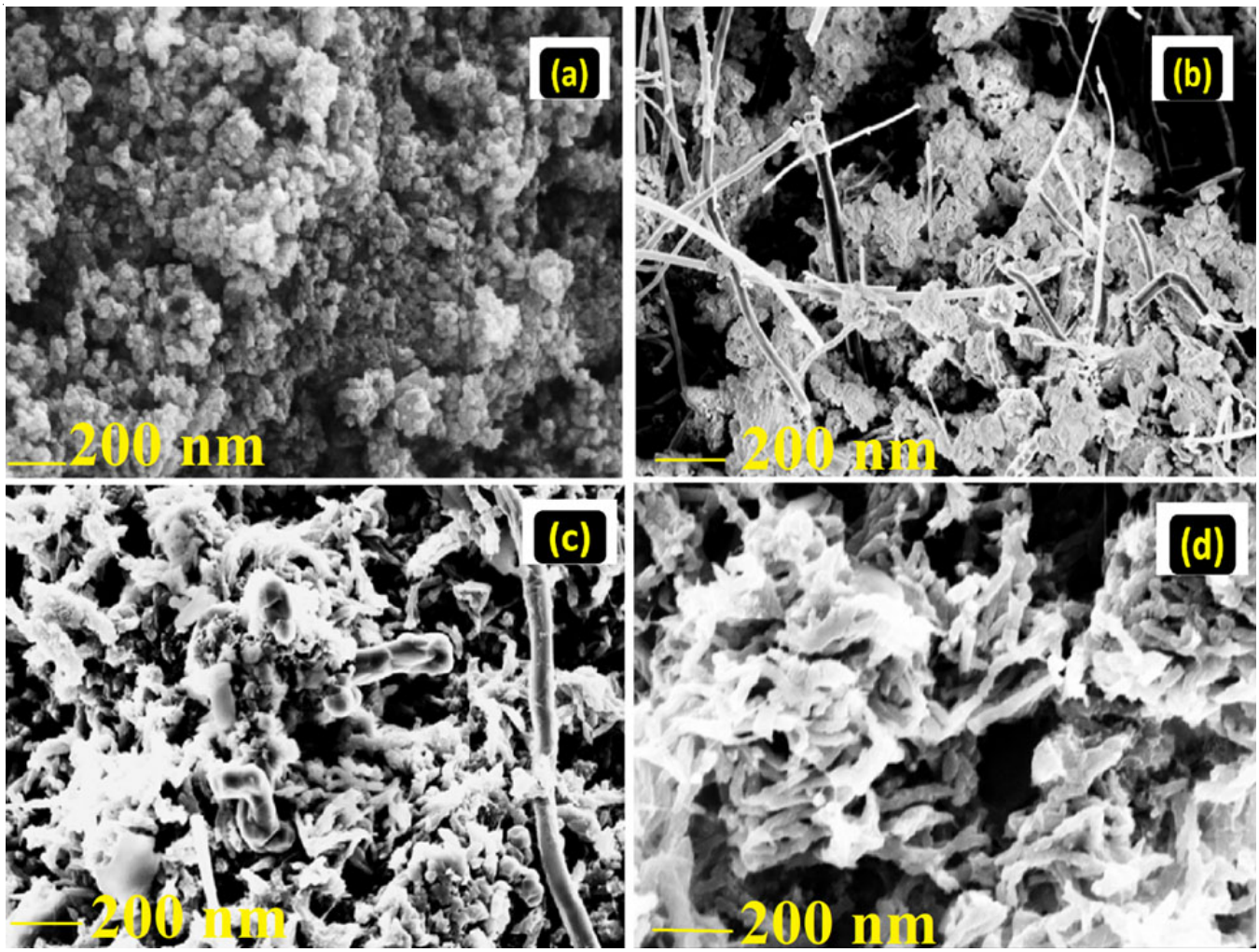

Fig. 5. FESEM micrographs of (a) MO, (b) CF, (c) PF and (d) CFP composites

depicted the surface morphology of CF. Formation of cobalt ferrite on the surface of CNF is observed, but two separate phases are visible. The FESEM image of PF in Fig. 5c indicates fibrous morphology. Coating of PANI upon carbon nanofiber surface is also clearly revealed. Surface modification of carbon nanofiber with acid treatment leads to the formation of functional groups, which act as active sites for nucleation and further growth of cobalt ferrite and PANI. A uniform and well aligned morphology is depicted for CFP in Fig. 5d.

From FESEM micrographs, it is observed clearly that PANI is uniformly wrapped over binary CF after oxidative polymerization of aniline. Such a uniform morphology could provide long diffusion path and easy electrolyte access. The bulk morphology of composite CFP was further analyzed with HRTEM in Fig. 7, which also confirms an intimate contact between PANI wrapped binary CF. Average diameter of coated CNF is about 14 nm and fringe spacing of lattice given 0.25 nm are clearly visible. Additionally, SAED pattern of corresponding space given in Fig. 7d indicates the polycrystalline nature of composite and well defined diffraction rings are consistent with the XRD results [47]. EDX analysis (Fig. 6) confirms the presence of Co, Fe and Mn metallic ions in the composites. Also, it is clear that no extra impurities are present in the composites.

Electrochemical studies: To explore the capacitive proficiency of such developed substances as active materials for electrodes, cyclic voltammetry, galvanostatic charging and discharging and EIS analysis were made in a system composed of three-electrodes at 5 mV s^{-1} with a potential scan rate range varying from (-0.1 to 0.9 V) in 1 M H_2SO_4. Cyclic voltammetry curves (CV) of MO, CF, PF and CFP are shown in Fig. 8a. In the CV curve of MO, a redox peaks pair is observed which indicates the pseudo-capacitance behaviour of cobalt ferrite [21]. The curve in binary CF becomes nearly rectangular referred as characteristic aspect of double-layer capacitance of carbon materials. The CV curve of PF shows a pair of redox peaks because of redox transition of PANI involving a semi-conducting leuco-emeraldine state and a conductingemeraldine form [48,49]. The CV curve of composite CFP exhibits two prominent redox peaks originating from the combined pseudocapacitance of cobalt ferrite as well as PANI. It is apparent that the composite CFP exhibits the current to the maximum and relatively larger curve area amongst the reported materials in this work, depicting its enhanced electrochemical conduct. The computed specific capacitances were from the CVs studies given as per the following equation:

$$C_s = \frac{I}{m} \times v \quad (1)$$

where C_s represents the specific capacitance (F g^{-1}), m for electrode material mass (g), I is given for the amperic current,

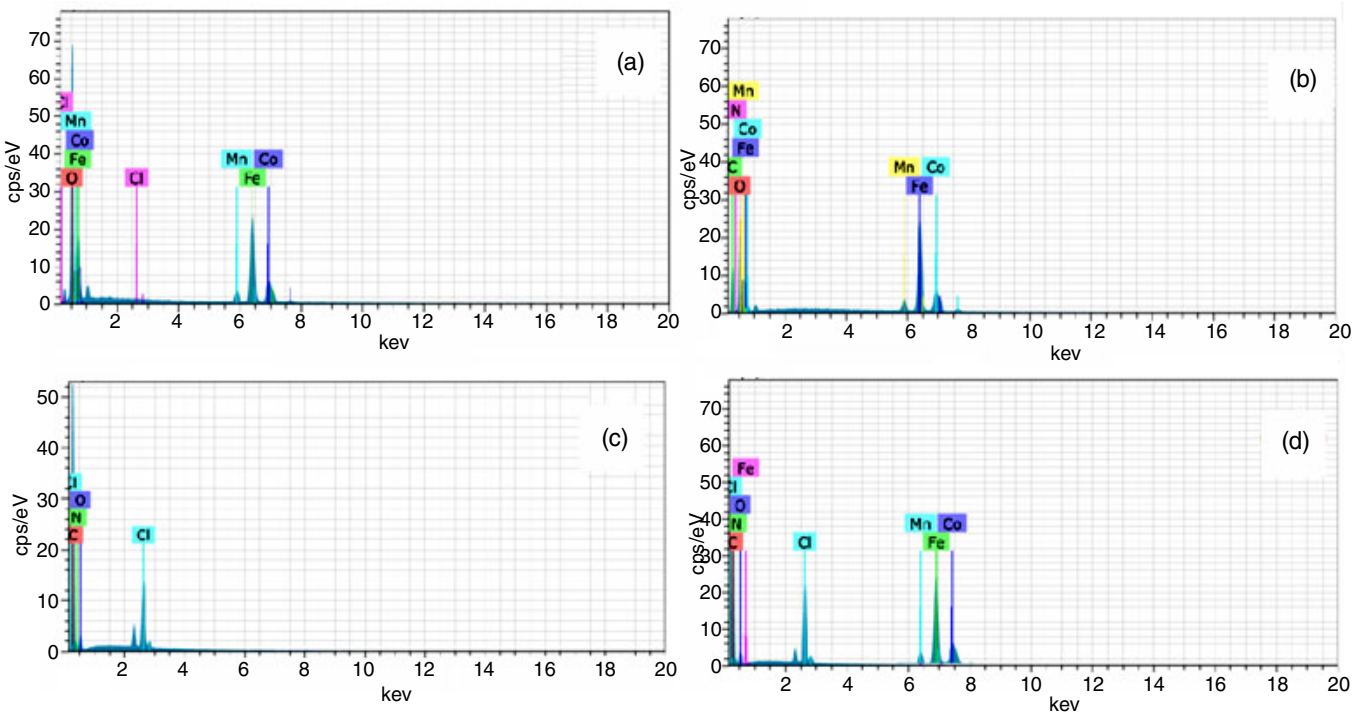

Fig. 6. EDS spectra of (a) MO, (b) CF, (c) PF and (d) CFP composites

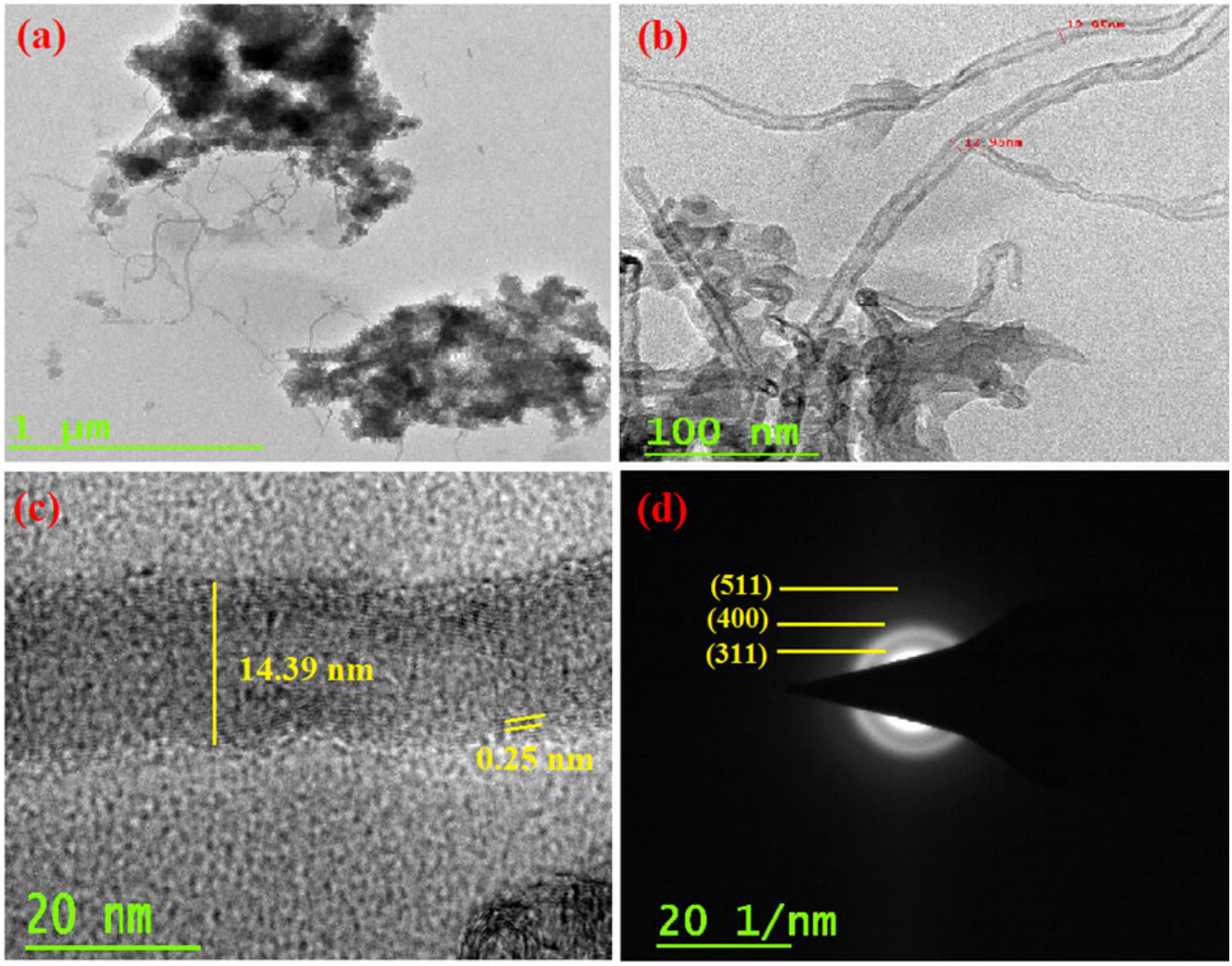

Fig. 7. HRTEM micrographs and (d) SAED pattern of CFP composite

considered as the average of oxidation current peak and reduction current peak and v is the symbol for scan rate in mV s^{-1}. Electrode materials MO, CF, PF and CFP exhibit 56, 266, 560 and 1860 F g^{-1} values for specific capacitance, respectively. This enhancement in the capacitive performance of composites while compared with PANI is recognized to the synergized input of all the components of electrode. The formation of nano-scaled cobalt ferrite layers onto the surface of carbon nanofiber credits an enhanced specific surface area and upgraded electrical contribution in comparison to the spherical particles of MO, facilitating easy and fast penetration of electrolyte ions. Manganese(II) ions exhibit variable oxidation states than the other two metal ions and also Mn supply lower redox potential, hence the swapping of Mn for Co in the spinel lattice facilitates an augmented charge exchange that prompts to eloquent enrichment in capacitance behavior in the composite [50]. Moreover, the availability of polar nitrogen groups by PANI layer boosts the wettability between the electrode and electrolyte and causes highly pseudo-capacitive reaction as because of the cobalt ferrite and nitrogen groups. The carbon nanofibers contributes electric double capacitance and provides mechanical strength to the composite material. Fig. 8b represents the volumetric curves of CFP at different scan rates. It is notable that the gross peak current goes high with rising potential scan rate, depicting its appreciable rate property and outstanding capacitance nature. To probe the capacitive aspects of composites, galvanostatic charge-discharge assessment were done in 1 M H_2SO_4.

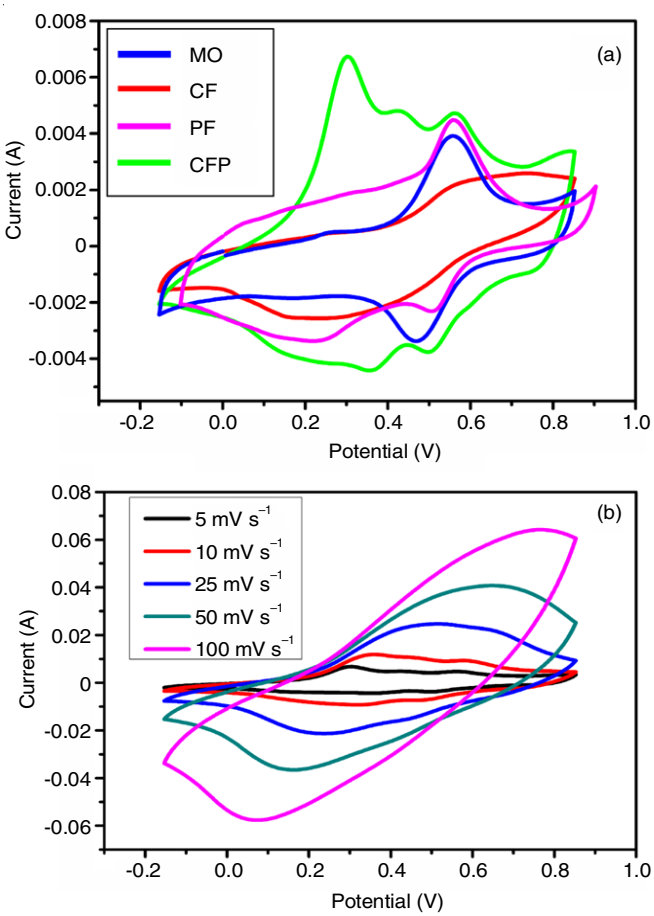

Fig. 8. CVs of (a) MO, CF, PF and CFP composites at 5 mV s^{-1} and (b) CFP at different scan rates

Fig. 9a shows the charging followed by discharging curves of electrode materials at 0.75 A g^{-1}. For composite PF and CFP non-linear curves occurred shows both pseudocapacitance and double layer capacitance nature attributed from the various constituent units of the composites. MO and CF display almost linear curves. The charging curve is symmetric relative to counterpart discharge and an accountable factor for an supreme super-capacitor. CFP presented the lowest voltage drop illustrating low internal resistance in the composites. The specific capacitances are computed using the equation given below:

$$C_{sp} = \frac{I \times \Delta t}{\Delta V \times m} \quad (2)$$

where C_{sp} denotes the specific capacitance in F g^{-1}, I for the current in Å, Δt refers to the discharge time given in seconds, m is the electrode material mass in grams and ΔV is symbol for the potential range in the course of discharge in volts. The highest discharge time span has been noted for CFP that explains it has the best electrochemical performance. The observed specific capacitances are 48, 185, 330 and 1450 F g^{-1} for MO, CF, PF and CFP, respectively. The outcome of charge discharge investigations are in agreement with cyclic voltammetry results. The CFP composite was further worked out at diverse current densities of 0.75, 1.0 and 1.5 A g^{-1} and the obtained graph is illustrated in Fig. 9b. It was found that charging-discharging curves continue to have a analogous shape at various current densities and coulombic efficiency is measured out to be nearly 98 %, inferring the sustainable nature of the composite [51]. The obtained specific capacitances values are 1450, 952 and 730 F g^{-1} at current density 0.75, 1.0 and 1.5 A g^{-1}, respectively.

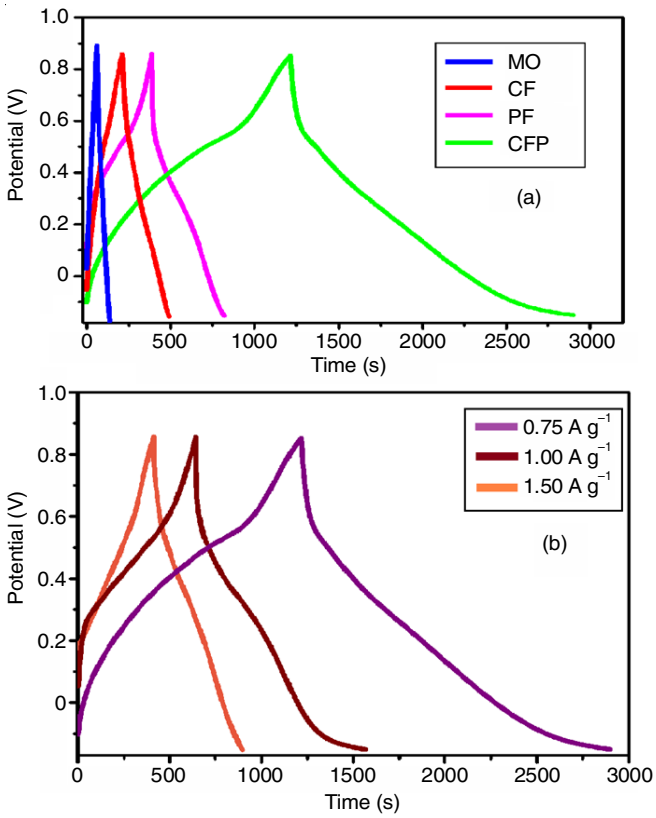

Fig. 9. Charge-discharge curves of (a) MO, CF, PF and CFP compositesat 0.75 A g^{-1} and (b) CFP atdifferent current densities

For an electrode material to be suitable for use in a energy storage device its stability and reversibility are two major attributes. Therefore, CFP electrode has been subjected to charge-discharge cycle test at 0.75 A g^{-1} current density to inspect it for its stability. After 500 cycles, the CFP electrode retained 85 % of initial specific capacitance demonstrating its lengthened cycle stability (Fig. 10). This was attained as result of conscious uniform coating of PANI over binary CF surfaces that improve the cycle stability of pseudo-capacitance by increased active sites.

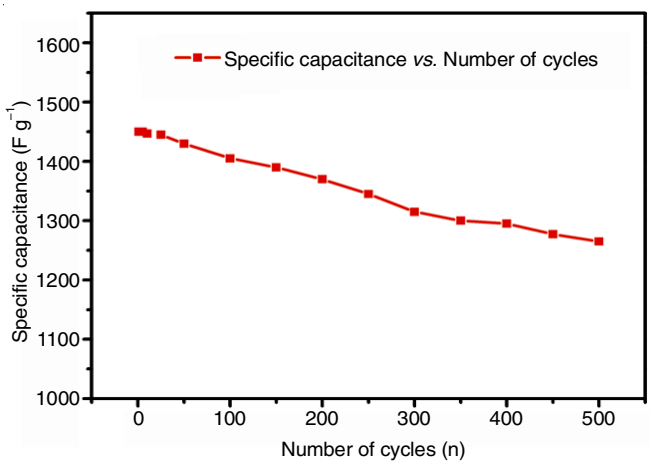

Fig. 10. Cycling performance of CFP composite at a current density of 0.75 A g^{-1}

Impedance spectroscopy (EIS) was applied to check the conductive attributes of the electrode. Fig. 11 shows the Nyquist graphs between Z′ and -Z″ plotted from 1Hz-100 kHz frequency range. Interception on X-axis gives an assessment of the equivalent series resistance or solution resistance (R_s). The composite posses a small X-axis intercept and a minimal semicircle signifying low internal resistance of composites. The suitable equivalent circuit was fixed for whole of the electrode stuff. The R_s values for composites MO, CF, PF and CFP electrodes are 1.71, 1.2, 2.1,1.25 Ω, respectively. The minimum value of R_s is reported for CFP among the various composites which is in consensus with the CV and charge-discharge findings and infer the superiority in terms of conductivity of the composites. At the low frequency rate, the reported composites displayed a higher vertical line containing slope near to 90º which also signifies the effortless ingress of electrolyte ions to the functional material and hence decreased resistance.

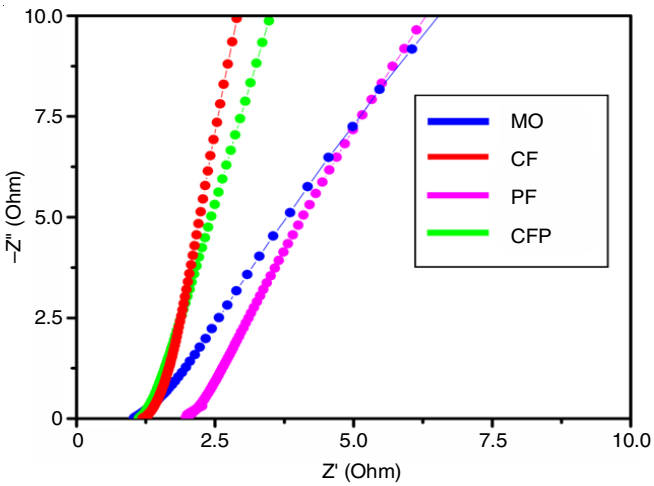

Fig. 11. Nyquist plots of MO, CF, PF and CFPcomposites

Conclusion

A novel electrode is fabricated with PANI/spinel metal oxide/carbon nanofiber (CFP) composite synthesized by combining hydrothermal method with *in situ* oxidative chemical polymerization route. The cell assembled with CFP electrode exhibits improved specific capacitance of 1860 F g^{-1} at a scan rate of 5 mV s^{-1} with a minimum solution resistance of 1.2 Ω that is significantly higher than those of pure spinel metal oxide, binary PANI/carbon nanofiber and binary spinel metal oxide/CNF composites. In CFP electrodes, the inner matrix of carbon nanofibers act as a double layer capacitor and outer conductive matrix of spinel metal oxide rich in oxygen ion concentration and PANI generates high pseudo-capacitance, which leads to such enhanced electrochemical attributes in CFP. The CFP also displays high reversibility and good retention (~85 %) in initial specific capacitance after 500 cycles.

ACKNOWLEDGEMENTS

The authors are grateful for the financial assistance in the form of major research project from TDT Division of Department of Science & Technology, Government of India (DST Ref. No: DST/TSG/PT/2009/116-G).

CONFLICT OF INTEREST

The authors declare that there is no conflict of interests regarding the publication of this article.

REFERENCES

1. Y. Huang, H. Li, Z. Wang, M. Zhu, Z. Pei, Q. Xue, Y. Huang and C. Zhi, *Nano Energy*, **22**, 422 (2016); https://doi.org/10.1016/j.nanoen.2016.02.047.
2. G. Wang, L. Zhang and J. Zhang, *Chem. Soc. Rev.*, **41**, 797 (2012); https://doi.org/10.1039/C1CS15060J.
3. S. Bhadra, D. Khastgir, N.K. Singha and J.H. Lee, *Prog. Polym. Sci.*, **34**, 783 (2009); https://doi.org/10.1016/j.progpolymsci.2009.04.003.
4. P. Liu and L. Zhang, *Crit. Rev. Solid State Mater. Sci.*, **34**, 75 (2009); https://doi.org/10.1080/10408430902875968.
5. D. Coltevieille, A. Le Méhauté, C. Challioui, P. Mirebeau and J.N. Demay, *Synth. Metals*, **101**, 703 (1999); https://doi.org/10.1016/S0379-6779(98)01093-5.
6. Zh.A. Boeva and V.G. Sergeyev, *Polym. Sci. Ser. C*, **56**, 144 (2014); https://doi.org/10.1134/S1811238214010032.
7. S. Ameen, M.S. Akhtar and M. Husain, *Sci. Adv. Mater.*, **2**, 441 (2010); https://doi.org/10.1166/sam.2010.1126.
8. J. Wang and D. Zhang, *Polym. Adv. Technol.*, **32(S1)**, E323 (2013); https://doi.org/10.1002/adv.21283.
9. Z. Lei, Z. Chen and X.S. Zhao, *J. Phys. Chem. C*, **114**, 19867 (2010); https://doi.org/10.1021/jp1084026.
10. P. Lu, D. Xue, H. Yang and Y. Liu, *Int. J. Smart Nano Mater.*, **4**, 2 (2013); https://doi.org/10.1080/19475411.2011.652218.
11. M. Sarfraz, M.F.A. Aboud and I. Shakir, *J. Alloys Compd.*, **650**, 123 (2015); https://doi.org/10.1016/j.jallcom.2015.07.274.
12. A.A. Ensafi, N. Ahmadi and B. Rezaei, *J. Alloys Compd.*, **652**, 39 (2015); https://doi.org/10.1016/j.jallcom.2015.08.226..
13. J. Chen, *J. Electrochem. Soc.*, **146**, 3606 (1999); https://doi.org/10.1149/1.1392522.

14. M.C. Liu, L.B. Kong, C. Lu, X.M. Li, Y.C. Luo and L. Kang, *ACS Appl. Mater. Interfaces*, **4**, 4631 (2012); https://doi.org/10.1021/am301010u.
15. T. Zhu, J.S. Chen and X.W. Lou, *J. Mater. Chem.*, **20**, 7015 (2010); https://doi.org/10.1039/c0jm00867b.
16. Y. Zhu, Z. Wu, M. Jing, X. Jia and X. Ji, *Electrochim. Acta*, **178**, 153 (2015); https://doi.org/10.1016/j.electacta.2015.08.004.
17. S.-K. Chang, Z. Zainal, K.-B. Tan, N.A. Yusof, W.M.D. Wan Yusoff and S.R.S. Prabaharan, *Ceram. Int.*, **41**, 1 (2015); https://doi.org/10.1016/j.ceramint.2014.07.101.
18. H.W. Wang, Z.A. Hu, Y.Q. Chang, Y.L. Chen, H.Y. Wu, Z.Y. Zhang and Y.Y. Yang, *J. Mater. Chem.*, **21**, 10504 (2011); https://doi.org/10.1039/c1jm10758e.
19. Z. Fan, J. Chen, K. Cui, F. Sun, Y. Xu and Y. Kuang, *Electrochim. Acta*, **52**, 2959 (2007); https://doi.org/10.1016/j.electacta.2006.09.029.
20. H. Kuan-Xin, W. Quan-Fu, Z. Xiao-gang and W. Xin-Lei, *J. Electrochem. Soc.*, **153**, A1568 (2006); https://doi.org/10.1149/1.2208735.
21. D.H. Deng, H. Pang, J.M. Du, J.W. Deng, S.J. Li, J. Chen and J.S. Zhang, *Cryst. Res. Technol.*, **47**, 1032 (2012); https://doi.org/10.1002/crat.201200161.
22. R.I. Jaidev, R.I. Jafri, A.K. Mishra and S. Ramaprabhu, *J. Mater. Chem.*, **21**, 17601 (2011); https://doi.org/10.1039/c1jm13191e.
23. L.J. Sun, X.X. Liu, K.K.T. Lau, L. Chen and W.M. Gu, *Electrochim. Acta*, **53**, 3036 (2008); https://doi.org/10.1016/j.electacta.2007.11.034.
24. L. Zheng, Y. Xu, D. Jin and Y. Xie, *Chem. Asian J.*, **6**, 1505 (2011); https://doi.org/10.1002/asia.201000770.
25. S. Dhibar and C.K. Das, *J. Alloys Compd.*, **653**, 486 (2015); https://doi.org/10.1016/j.jallcom.2015.08.158.
26. R. Yuksel, C. Durucan and H.E. Unalan, *J. Alloys Compd.*, **658**, 183 (2016); https://doi.org/10.1016/j.jallcom.2015.10.216.
27. V.V. Abalyaeva, G.V. Nikolaeva and O.N. Efimov, *Russ. J. Electrochem.*, **44**, 828 (2008); https://doi.org/10.1134/S1023193508070094.
28. L.-Y. Meng and S.-J. Park, *Carbon Lett.*, **15**, 89-104 (2014); https://doi.org/10.5714/CL.2014.15.2.089.
29. I. Kovalenko, D.G. Bucknall and G. Yushin, *Adv. Funct. Mater.*, **20**, 3979 (2010); https://doi.org/10.1002/adfm.201000906.
30. M.H. Al-Saleh and U. Sundararaj, *Carbon*, **47**, 2 (2009); https://doi.org/10.1016/j.carbon.2008.09.039.
31. L. Feng, N. Xie and J. Zhong, *Materials*, **7**, 3919 (2014); https://doi.org/10.3390/ma7053919.
32. A.M. Cojocariu, M. Soroceanu, L. Hrib, V. Nica and O.F. Caltun, *Mater. Chem. Phys.*, **135**, 728 (2012); https://doi.org/10.1016/j.matchemphys.2012.05.051.
33. T. Slatineanu, A.R. Iordan, M.N. Palamaru, O.F. Caltun, V. Gafton and L. Leontie, *Mater. Res. Bull.*, **46**, 1455 (2011); https://doi.org/10.1016/j.materresbull.2011.05.002.
34. H. Yan and K. Kou, *J. Mater. Sci.*, **49**, 1222 (2014); https://doi.org/10.1007/s10853-013-7804-9.
35. A.K. Sharma and Y. Sharma, *Anal. Lett.*, **45**, 2075 (2012); https://doi.org/10.1080/00032719.2012.680057.
36. W. Wu, Y. Li, L. Yang, Y. Ma and X. Yan, *Synth. Met.*, **193**, 48 (2014); https://doi.org/10.1016/j.synthmet.2014.03.029.
37. J. Yang, X. Wang, X. Wang, R. Jia and J. Huang, *J. Phys. Chem. Solids*, **71**, 448 (2010); https://doi.org/10.1016/j.jpcs.2009.12.008.
38. H. Liu, Y. Wang, X. Gou, T. Qi, J. Yang and Y. Ding, *Mater. Sci. Eng. B*, **178**, 293 (2013); https://doi.org/10.1016/j.mseb.2012.12.002.
39. X.S. Du, M. Xiao and Y.Z. Meng, *Eur. Polym. J.*, **40**, 1489 (2004); https://doi.org/10.1016/j.eurpolymj.2004.02.009.
40. J. Luo, Y. Xu and D. Gao, *Solid State Sci.*, **37**, 40 (2014); https://doi.org/10.1016/j.solidstatesciences.2014.08.007.
41. P.K. Upadhyay and A. Ahmad, *Chin. J. Polym. Sci.*, **28**, 191 (2010); https://doi.org/10.1007/s10118-010-9004-2.
42. C. Bora, A. Kalita, D. Das, S.K. Dolui and P.K. Mukhopadhyay, *Polym. Int.*, **63**, 445 (2014); https://doi.org/10.1002/pi.4522.
43. L.G. Toma and R.M. Ion, *J. Optoelectron. Adv. Mater.*, **12**, 2113 (2010).
44. R. Singhal and V. Kalra, *J. Mater. Chem. A Mater. Energy Sustain.*, **3**, 377 (2015); https://doi.org/10.1039/C4TA05121A.
45. D. Saini and T. Basu, *App. NanoSci.*, **2**, 467 (2012); https://doi.org/10.1007/s13204-012-0059-y.
46. N.T. Tung, T. Van Khai, M. Jeon, Y.J. Lee, H. Chung, J.-H. Bang and D. Sohn, *Macromol. Res.*, **19**, 203 (2011); https://doi.org/10.1007/s13233-011-0216-2.
47. C. Singh, A. Goyal and S. Singhal, *Nanoscale*, **6**, 7959 (2014); https://doi.org/10.1039/C4NR01730G.
48. E.M. Genies and M. Lapkowski, *J. Electroanal. Chem. Interfacial Electrochem.*, **220**, 67 (1987); https://doi.org/10.1016/0022-0728(87)88005-1.
49. Y.K. Zhou, B.L. He, W.J. Zhou, J. Huang, X.H. Li, B. Wu and H.L. Li, *Electrochim. Acta*, **49**, 257 (2004); https://doi.org/10.1016/j.electacta.2003.08.007.
50. S.K. Chang, K.T. Lee, Z. Zainal, K.B. Tan, N.A. Yusof, W.M.D.W. Yusoff, J.F. Lee and N.L. Wu, *Electrochim. Acta*, **67**, 67 (2012); https://doi.org/10.1016/j.electacta.2012.02.014.
51. P. Xiong, C. Hu, Y. Fan, W. Zhang, J. Zhu and X. Wang, *J. Power Sources*, **266**, 384 (2014); https://doi.org/10.1016/j.jpowsour.2014.05.048.